

Article

Design and Test of an Arc-Shaped Tooth Press Device for Combined Soil Preparation Equipment for Growing Potatoes

Zhiming Zhao , Xiaoxin Zhu, Jicheng Li * , Jinqing Lyu, Yu Qi and Jinni Liu

College of Engineering, Northeast Agricultural University, Harbin 150030, China; zzm000420@163.com (Z.Z.); neau_zxx@163.com (X.Z.); lj888886666@163.com (J.L.); qiyu_1999@163.com (Y.Q.); 18204585479@163.com (J.L.)
* Correspondence: leejc@neau.edu.cn; Tel.: +86-0451-55190667

Abstract: In response to the low soil breakage rate and poor flatness of current combined soil preparation equipment for growing potatoes under the clay loam conditions of Northeast China, this paper presents the design of an arc-shaped tooth press device for such equipment, describing its overall structure and working principle. By conducting force analysis on the press roller and shear stress analysis with MATLAB, we obtained the structural parameters and the corresponding value ranges impacting the operational effectiveness of the press device. A three-factor, five-level quadratic regression orthogonal rotational combination test was carried out using EDEM discrete element simulation software, taking the soil breakage rate and flatness as the test indicators. The forward speed, roller tooth arc length, and angle between the roller tooth and the vertical direction (ABRTVD) were the test factors. Design-Expert 8.0.6 software was used for data processing and analysis, and the results showed that the optimal parameter combination consisted of a forward speed of $0.72\sim 1.15\text{ m}\cdot\text{s}^{-1}$, a roller tooth arc length of 58.7 mm, and an ABRTVD of 37.74° , at which point the soil breakage rate was 93.58% and the flatness value was 21.36 mm. The optimal combination of parameters was selected for the field test, resulting in a soil breakage rate of 95.6% and a flatness value of 20.6 mm. The results of the simulation test were found to be consistent with the field test results, thus validating the efficacy of the device design. The findings of this study can provide a reference for enhancing the operational performance of combined soil preparation equipment for growing potatoes under clay loam conditions.



Citation: Zhao, Z.; Zhu, X.; Li, J.; Lyu, J.; Qi, Y.; Liu, J. Design and Test of an Arc-Shaped Tooth Press Device for Combined Soil Preparation Equipment for Growing Potatoes. *Agriculture* **2023**, *13*, 1193. <https://doi.org/10.3390/agriculture13061193>

Academic Editors: Zhongbing Chen, Safdar Bashir and Saqib Bashir

Received: 4 May 2023

Revised: 21 May 2023

Accepted: 23 May 2023

Published: 3 June 2023



Copyright: © 2023 by the authors. Licensee MDPI, Basel, Switzerland. This article is an open access article distributed under the terms and conditions of the Creative Commons Attribution (CC BY) license (<https://creativecommons.org/licenses/by/4.0/>).

Keywords: combined soil preparation equipment; arc-shaped tooth; press device; discrete element method; design and test

1. Introduction

The quality of potato sowing and the subsequent emergence of seedlings is contingent upon the degree to which the soil was adequately prepared prior to planting. One of the most critical factors for increasing potato yields is ensuring that the soil is loose and flat before sowing [1–4]. Pre-sowing soil preparation for potatoes can enhance the soil's water storage and preservation capacity, increase the soil's moisture content, improve the soil's grain structure, and augment the crop's ability to adapt and regulate under natural conditions [5–7]. The press device determines the operation effect of combined soil preparation equipment for potatoes, which is related to whether the whole device can fulfil its purpose of pressing, ensuring flatness, and breaking the soil. Currently, the existing research on combined soil preparation equipment mainly focuses on designing soil-crushing devices and analyzing the combined parameters within small-scale tests, thus improving the soil breakage rate and reducing energy consumption. However, there is less research into the press device's impact on the flatness and degree of secondary crushing of soil. Therefore, it is essential to study highly efficient combined soil preparation equipment for growing potatoes when using a press device to improve the soil breakage rate and soil flatness, such that the potato yield can be increased.

Matin et al. [8] focused on designing and optimizing parameter combinations for rotary tillage knives working specifically with wet clay soils in Asia, while only using cylindrical press devices, which was not conducive to improving the breakage rate or the flatness of soil preparation completed by the machine. Lee et al. [9] researched the impact of rotating blade shape, rotation direction, and number of peripheral rotating blades on strip tillage characteristics; however, the soil flatness after operation was not investigated. Zhao et al. [10] designed combined soil preparation equipment with a cage-shredding roller for broken soil after rototilling, but this resulted in the formation of empty holes with low compactness, which is not conducive to the emergence of potatoes. Kang et al. [11] developed a deep, loosening, and stubble-breaking-combined soil tillage machine, which made the soil finely crushed and evenly granulated and increased the soil density; however, its press rollers were formed of equally spaced welded circles with gaps in the middle, which are not suitable for the clay loam in Northeast China. Chen et al. [12] developed a counter-roller squeeze-type tide soil preparation machine. It was designed with three different rectangular roller teeth and installed using a counter-roller squeeze. Dai et al. [13] designed a monopoly-shaping press device that met the requirements for the agronomical technology of dryland full-film mulching surface planting, analyzed its relevant parameters, and determined good operating parameters. Zhao et al. [14] designed a press device capable of bi-directional shaping and adjustable press strength to address the problems of uneven pressurization and insufficient strength in hills. This machine was unsuitable for clay loam because it resulted in a lower breakage rate of soil and caused soil adhesion to the roller tooth, which is not conducive to the machine's normal operation.

Using the discrete element method (DEM) to study the action of land preparation implements on the soil can save time and reduce the cost of experiments. Hence, this paper presents an EDEM simulation of the suppression device based on theoretical analysis. Okayasu et al. [15] conducted a modeling study on soil adhesion power that simulated natural clay loam by introducing parallel bonds between particles. The simulation results showed that the parallel-bonding bond model was closer to the actual soil particles. Kim et al. [16] analyzed the impact of tillage depth on traction under clay loam conditions using EDEM software. Zhang et al. [17] investigated the triaxial resistance of a rotary tillage knife by modifying its structural parameters to research energy consumption during operation. Barbosa et al. [18] developed different tillage implements and utilized EDEM software to establish the agglomerate structure of block soils. Energy consumption can be calculated during operation in order to create a tillage implement with minimal energy expenditure. Du et al. [19] performed a theoretical analysis of the rotary tiller and validated it through discrete element simulation. The results showed that the research method is highly feasible. The above research results provide references for the utilization of the DEM in analyzing the properties of clay loam. Based on the theoretical analysis, simulation using the DEM is reliable and provides a reference for the research in this paper.

2. Materials and Methods

2.1. Design of the Press Device

2.1.1. Structure and Operation Principle

The technical parameters and overall structure of the press device—i.e., a piece of combined soil preparation equipment for growing potatoes—studied in this paper are shown in Table 1 and Figure 1a, respectively. The machine is mainly composed of a transmission device, upper link device, suspension device, deep loosening device, soil breakage device, press device, and soil scraping device. The machine is linked to the tractor via the suspension device; the deep loosening device installed at the front of the machine breaks the plough pan; the transmission device provides power to the soil breakage device for the soil-cutting operation; and the press device further breaks, compacts, and levels the soil thrown by the soil breakage device.

Table 1. Technical parameters of the press device.

Parameter	Value	Unit
Press device overall dimensions (length × width × height)	700 × 2400 × 1150	mm × mm × mm
Matching power	≥55	kW
Connection method	Three-point suspension	/
Working width	2200	mm
Working speed	2.5~4	km/h

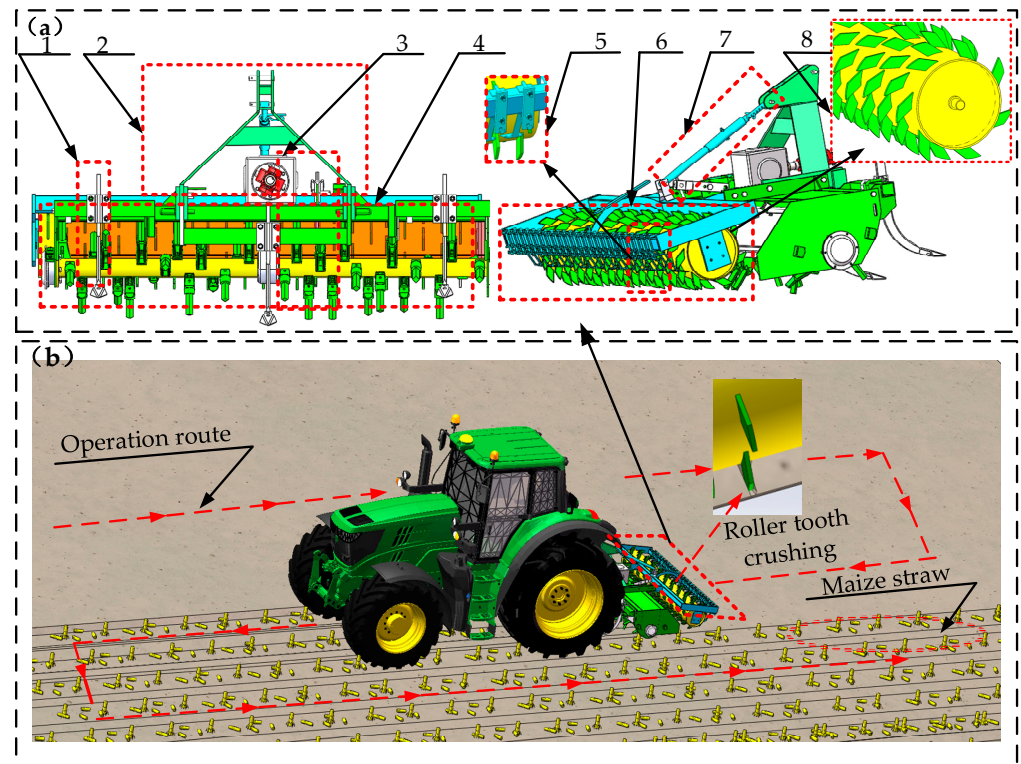


Figure 1. (a) Overall structure of the combined soil preparation equipment: 1. Deep loosening device; 2. suspension device; 3. transmission device; 4. soil-breakage device; 5. soil-scraping device; 6. press device; 7. upper link device; and 8. press device. (b) Combined soil preparation equipment operating condition.

The working principle and technical characteristics of the combined soil preparation equipment for growing potatoes are shown in Figure 1b. When the combined soil preparation equipment works, it mainly breaks the previous crop's stubble and surface soil. During the operation, the tractor drives forward with the soil preparation equipment, in which the soil breakage device breaks up large pieces of soil and throws them toward the broken baffle behind, further breaking the soil in the collision process; the arc-shaped tooth press device is attached to the front of soil breakage device by an upper link device, and at the same time, the soil thrown over by the soil breakage device is further finely crushed, leveled, and pressed. To enhance the soil breaking performance of the press device, six arc-shaped teeth rollers were welded evenly in each cross section at equal intervals in the direction of the press roller axis, and the soil was crushed and flattened during the operation. To avoid the soil congestion and obstruction caused by soil adhering to the press roller, a soil-scraping device was installed on the back beam of the press roller. At the end of the machine's work, it is capable of achieving a soil structure that is loose at the top and solid at the bottom, thus meeting the needs of potatoes before sowing.

2.1.2. Key Component Design

The press device is a crucial component of the combined soil preparation equipment, as it can form a soil layer structure with compacted topsoil and loose subsoil, and its performance has a direct impact on the operational effectiveness of the entire machine. Therefore, the design and analysis of the working process and structure of the press device are required. In northeast China, the soils are highly cohesive, and, with strong tillage resistance and poor tillage performance, the design of the press device needs to be combined with the agronomic requirements prior to potato sowing. That is, in the operating process, the soil can be further broken, compacted, and leveled, and the press roller does not adhere to the soil, which meets the requirements of soil fragmentation and flatness for potato sowing.

Press roller is the key component of the press device, and its parameters need to be designed. Under the same weight, the smaller the diameter and width of the press roller, the greater the rolling resistance. The diameter of the press roller has a much more significant effect on rolling resistance than its width, increasing the diameter of the press roller not only can decrease the rolling resistance, but also reduces the slip and congestion resistance [20,21]. However, the excessive diameter of the press roller will affect the machine's overall stability and increase the manufacturing costs. In this paper, to ensure working strength and to reduce the rolling resistance of the press roller, a mathematical model for soil resistance during the movement of the press roller is established. Under the working condition of the press roller, the process of soil force and deformation is more complex; thus, the motion of the press roller relative to the soil is analyzed by a static model, and the velocity variable is introduced during the movement of the press roller. A rectangular coordinate system was established, as shown in Figure 2, taking the center of the press roller as the coordinate origin O , the forward direction of the press roller as the positive x -axis, and the vertically downward direction as the positive y -axis.

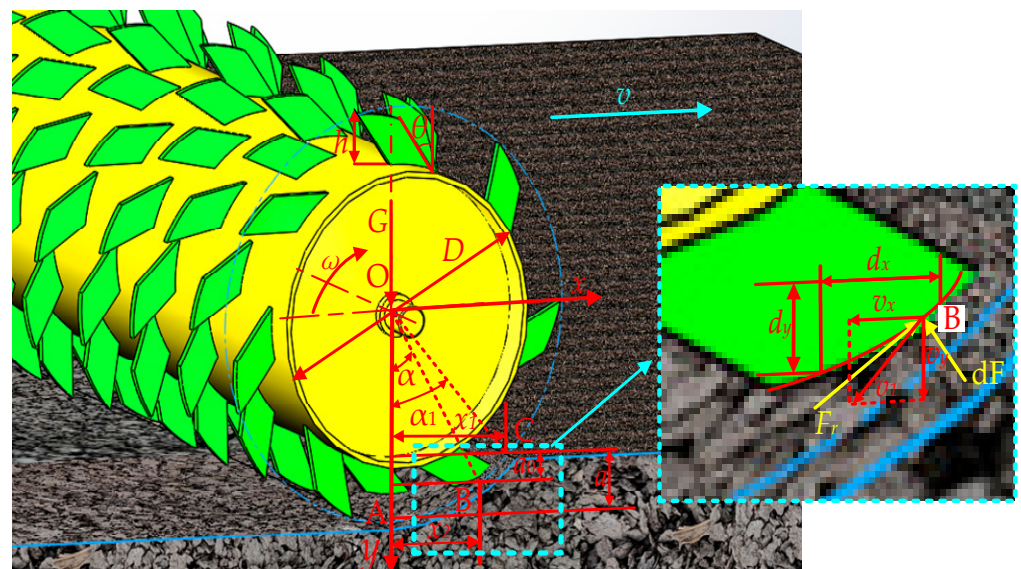


Figure 2. Analysis of forces on roller teeth. Note: A is the point at which the roller tooth leaves the soil, B is a point during the action of the roller tooth, C is the point at which the roller tooth first acts on the soil, D is the diameter of the press roller, O is the origin of the coordinates, and G is the gravity of the press roller.

The vertical component of the compressive reaction force of soil on the arc surface ABC of the press roller tooth is equal to the gravity of the crushing roller itself, G . Take a

tiny arc segment ds at point B , which can be approximated as a straight-line segment, and the total reaction force of the roller tooth touching the soil arc surface ABC is obtained as:

$$\int_0^{x_1} pb \cos^2 \alpha dx = G \tag{1}$$

where x_1 represents the horizontal coordinate value between points A and C , mm; p is the compressive strength of the soil, kPa; b is the width of the press roller, mm; α is the angle corresponding to the press depth a , °; and G is the gravity of the press roller itself, N.

The compressive strength of the soil is not only related to the velocity v_1 here, but also to the static modulus of soil deformation, soil deformation index, and velocity change index, which can be obtained from the base point method:

$$v_1 = \frac{2x_1v}{D + 2h} \tag{2}$$

where D is the diameter of the roller, mm; h is the height of the press roller tooth, mm.

Referring to the geometric relationship, when determining the equation between x_1 and a_0 , the compaction depth difference ($a - a_0$) is small and negligible compared to the diameter of the press roller. The compressive reaction force is obtained as:

$$\int_0^{x_1} k_0 \left(\frac{2x_1v}{D + 2h} \right)^m \left(a - \frac{x_1^2}{D + 2h} \right)^n (\cos^2 \alpha) b dx = G \tag{3}$$

where k_0 is the static modulus of the soil when deformation occurs; m is the velocity change index; n is the deformation index of soil; and a is the compaction depth at point A , mm.

Since Equation (3) contains two variables, x_1 and a_0 , it cannot be solved directly by integrating. Therefore, the term $\left(a - \frac{x_1^2}{D + 2h} \right)^n$ is expanded in an infinite series, by integrating its first two terms, and a functional relationship between press depth and diameter of the press roller can be derived. Through the empirical formulas of simultaneous press roller design, we can obtain the following:

$$\begin{cases} a = \left[\frac{G}{2^{\frac{m+1}{2}} v^m k_0 b \left(\frac{D}{2} + h \right)^{\frac{1-m}{2}} \left(\frac{1}{m+1} - \frac{n}{m+3} \right)} \right]^{\frac{2}{2n+m+1}} \\ D + 2h = \frac{2 \times a}{1 - \cos \alpha} \end{cases} \tag{4}$$

By consulting the agricultural machinery design manual, it can be seen that the diameter of the press roller for field operation ranges from 300 to 700 mm. By solving Equation (4), the diameter of the press roller is selected as 325 mm, and the height of the roller tooth as 70 mm.

For the clay loam of northeast China, the soil breakage device only partially breaks up the clods after working, and the clods tend to form hollows when they accumulate, which is not conducive to the germination of seed potatoes at a later stage [22]. To solve this problem, arc-shaped roller teeth are welded onto the press roller to further finely crush the soil thrown backward by the soil breakage device, thus increasing the fine-crushing capacity of the whole device for soil. Meanwhile, by twice considering the impact of the press roller on soil flatness during breaking soil, the end surface of the roller tooth was designed as an arc shape, and the curvature of the roller tooth was made same as that of the press roller.




The thickness of the roller tooth was calculated by an empirical formula:

$$S = f \times (D + 2h) \tag{5}$$

where S is the thickness of the roller tooth, mm; f is the thickness factor, and the value range is 0.008~0.02 [23].

The thickness range of the roller tooth was calculated to 3.72~9.3 mm. To improve the wear resistance of the roller tooth and to take into account the thickness of standard steel plates during processing, the final thickness of the tooth was determined to be 8 mm. The clods were split into three levels based on the length of the longest side of clods after the combined soil preparation equipment had completed its operation, as illustrated in Table 2. To improve the soil breakage rate of machine and to avoid clogging between the roller teeth, the distance between the roller teeth was set to 70 mm.

Table 2. Clod size classification.

Type	Size and Scale
Small clods	 $40 \text{ mm} \leq$ $60 \sim 75\%$
Middle clods	 $40 \sim 80 \text{ mm}$ $10 \sim 30\%$
Large clods	 $\geq 80 \text{ mm}$ $10 \sim 15\%$

Soil-cutting resistance primarily depends on the soil shear strength, which not only depends on the macroscopic physical properties of the soil, but also on the environment in which it is located [24]. Lapen et al. found that soil-cutting resistance was positively correlated with soil type and soil moisture content [25]. In the process of a press roller operation, as the machine moves forward, the roller tooth cuts into soil under the action of forces, such as gravity and cutting force, and breaks it up. The cutting force is generated through the forward rotational movement of the press roller, which is driven by tractor traction. If the roller tooth can break the soil, the shear stress of the roller tooth on the soil should be greater than the shear strength of the soil, i.e., the following relationship is satisfied:

$$\begin{cases} F_r = \frac{2K_r \pi v^2 \cos^2 \omega t}{\sqrt{\lambda^2 + 1} - 2\lambda \sin \omega t \sqrt{2 + 2 \sin \omega t}} \\ G_C = \frac{G}{n} \\ F_s = F_r + G_C \cos \theta \\ \frac{F_s}{S_l} > [\sigma] \end{cases} \quad (6)$$

where F_r is the cutting force of roller tooth on the soil, N; K_r is the resistance characteristic of the soil, $\text{kg}\cdot\text{m}^{-1}$; ω is the angular speed of the press roller, $\text{rad}\cdot\text{s}^{-1}$; t is the operating time, s; λ is the kinematic parameter of rotating machinery; G_C is the vertical force of gravity at point C, N; n is the number of tooth of the whole press roller touching the ground at this moment, N; S is the thickness of roller tooth, mm; and l is the arc length of the press roller tooth, mm.

As can be seen from Equation (6), the factors affecting the shear stress of the roller tooth are the following:

- The forward speed of the press roller;
- The roller tooth arc length;
- The angle between the roller tooth and the vertical direction (ABRTVD).

MATLAB 2019b (MathWorks. Inc., Natick, MA, USA) software was used to analyze the relationship between these three factors and the shear stress under clay loam conditions with a moisture content of 15%; the objective was to investigate whether the above factors could break up the soil, and to determine the range of parameters for each factor.

As can be seen from Figure 3a, the shear stress of the roller tooth can meet the requirements for the shredding soil that arises from the roller tooth cutting into the soil as they leave the soil, and the cutting stress of the roller tooth is positively correlated with time. In the range of $0.5\sim 1.5\text{ m}\cdot\text{s}^{-1}$ of forward speed, as the forward speed and the angular speed of the roller tooth rotation increase, the shear stress of the roller tooth also increases accordingly. From Figure 3b, it can be seen that the shear stress is greater than the shear strength of clay loam in the range of 54~60 mm of the roller tooth arc length (this can meet the performance requirements of the roller tooth breakage soil), and the shear stress decreases with the increasing of arc length. When the arc length remains constant, the shear stress decreases as the angle θ increases. The reason for this is that the component force on the soil of roller tooth's gravity decreases.

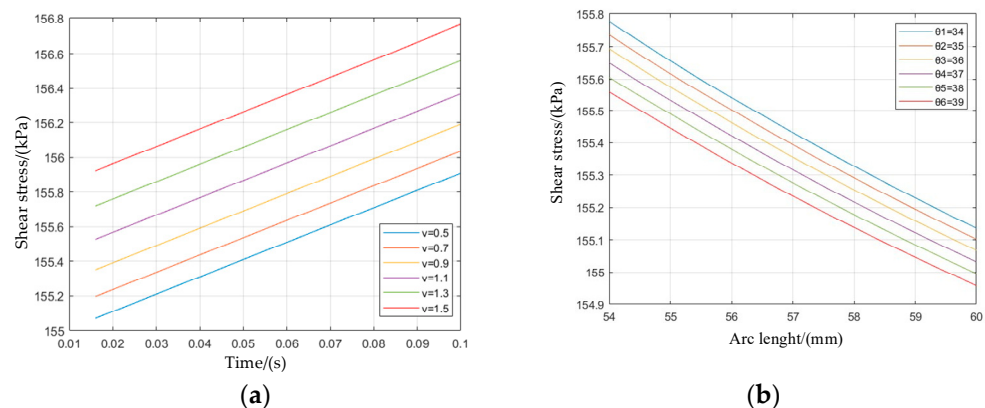


Figure 3. (a) Plot of shear stress versus time. (b) Plot of shear stress versus roller tooth arc length.

2.2. Methods

By analyzing the shear stress of the roller tooth, the operational parameters and structural parameters that affect the shear stress of press device were obtained. MATLAB software was used to analyze and obtain the value range of each parameter, the forward speed was $0.5\sim 1.5\text{ m}\cdot\text{s}^{-1}$, the arc length of roller tooth was 54~60 mm, and the ABRTVD was $34\sim 40^\circ$, respectively. The choice of operational and structural parameters significantly affects the breakage rate of soil and flatness. In order to improve the secondary soil breakage rate of the press device and the operation flatness after compacting, a discrete element simulation model of the press device operating on the soil was established by using EDEM software. The simulation optimization experimental study was carried out by combining the quadratic regression orthogonal rotating center combination test in order to obtain the optimal parameter combination [26].

2.2.1. Simulation Model Construction

The press device was modeled in an equal scale by using SolidWorks 2020 (Dassault Systèmes, Paris, France). Due to the large working width of the press device and the operation effect of the scraping device being unable to be tested in the simulation process, considering the computational capabilities of computer, only the press roller and its teeth were retained during the modeling process, and the length of the press roller was also appropriately reduced. The model was imported into the EDEM 2020 (Altair Engineering, Troy, MI, USA) software in (X_T) format, as shown in Figure 4a. According to the actual processing and production situation, the material of the press roller and its teeth were set to 65 Mn.

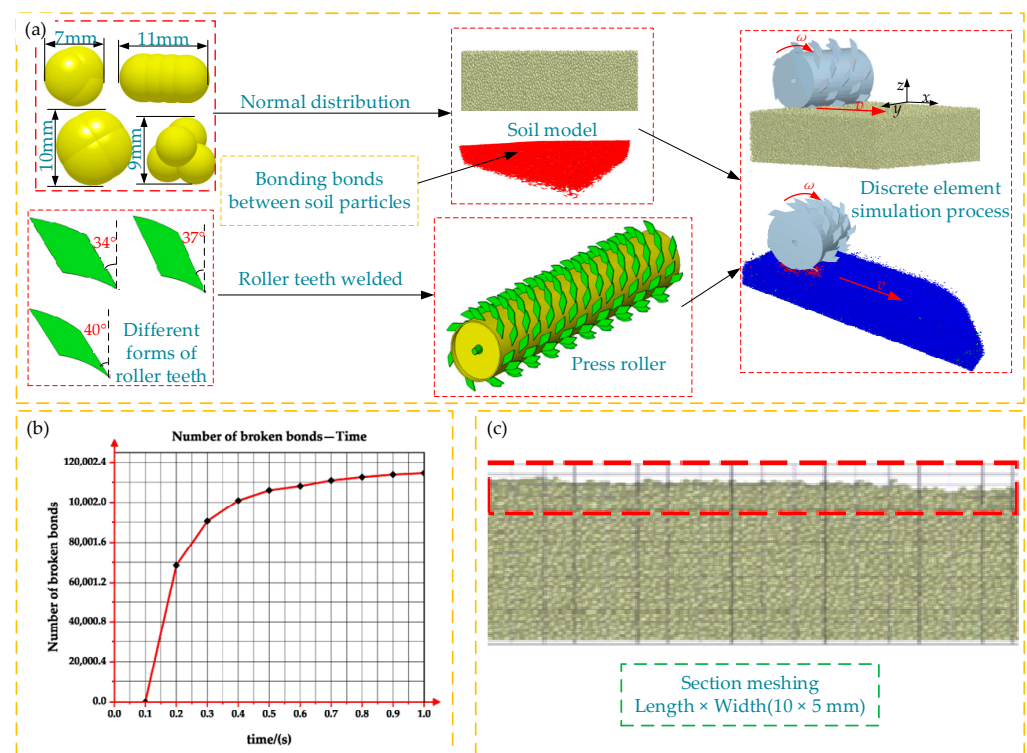


Figure 4. (a) Simulation flow chart; (b) Plot of time versus the number of particles breaking the bond; and (c) The cross-sectional view of flatness after operating.

For the structural characteristics of clay loam, the modeling of soil particles was performed using EDEM 2020 software, and the diameter of soil particles was set at 5 mm; the Hertz–Mindlin Bonding model was selected as the bonding model between particles, and the bonded radius was set as 5.5 mm [27,28]. The specific parameters are shown in Table 3. When the soil model was established, the diameter of soil particle was normally distributed, and the soil bin’s length, width, and height were 1000 mm, 1000 mm, and 600 mm, respectively. The soil model was generated in static mode and instantly filled the entire soil bin trough at the beginning of simulation. However, the distance between soil particles at that time was too large, which does not conform to the actual situation of clay loam. Therefore, a downward load was added above the soil bin model to make the soil sink and to reduce the distance between soil particles; the soil bulk density eventually reached $1.0\sim 1.5\text{ g}\cdot\text{cm}^{-3}$ and thus could achieve the requirements of clay loam.

Table 3. Bonded particle breakage model parameters.

Item	Value
Tangential shear modulus	5500
Normal modulus of elasticity	4000
Tangential maximum stress (N)	9000
Normal maximum stress (N)	4000
Radius of bonded particles (mm)	5.5

In order to enhance the effectiveness of the DEM simulation, it is crucial to choose suitable material contact models and correct edge parameters. The Hertz–Mindlin contact model was adopted between the soil and the press device. By consulting the relevant literature [29,30], the contact and intrinsic parameters of each material were obtained, as shown in Table 4. Material physical and contact mechanical properties parameters: The press device was installed at one end of the soil bin for initial operation. It was rotated clockwise around the y -axis, and the positive direction of the x -axis was the forward direction of press device, as shown in Figure 4a. A fixed time step of 5.76×10^{-5} s was used to perform the simulation, which is 10% of the Rayleigh time step. The cell grid size was set to three times the average particle diameter. The total duration of the simulation was 3 s, and the simulation data were saved every 0.05 s. To ensure the continuity of the simulated motion, only the test results for 1 s within the stable working interval were extracted for subsequent statistical analysis [31].

Table 4. Material physical and contact mechanical properties parameters.

Properties	65 Mn/Source	Soil/Source
Density/($\text{kg}\cdot\text{m}^{-3}$)	7800	2650
Shear's modulus/Pa	7.96×10^{10}	1.0×10^6
Poisson's ratio	0.3	0.34
Coefficient of rolling friction (to soil)	0.11	0.2
Coefficient of friction (to soil)	0.65	0.3
Coefficient of restitution (to soil)	0.6	0.6

2.2.2. Simulation Test Program

The test was carried out according to the standard GB/T 5668-2017 “Rotary Tiller”. The test factors that were selected were the forward speed, roller tooth arc length, and the ABRTVD. The breakage rate of soil and flatness were chosen as the simulation test indexes to evaluate the secondary soil crushing and compaction effect of the press device. A three-factor, five-level quadratic regression orthogonal rotated combination test was conducted to evaluate the press device's performance. The test factors were coded according to the level coding scheme presented in Table 5, and 23 parameter combinations were tested.

Table 5. Test factors coding.

Test Factors	Coded Value				
	−1.682	−1	0	1	1.682
x_1 Forward speed $v/(\text{m}\cdot\text{s}^{-1})$	0.16	0.5	1	1.5	1.84
x_2 Roller tooth arc length $l/(\text{mm})$	52	54	57	60	62
x_3 ABRTVD $\theta/(\text{°})$	32	34	37	40	42

The combination of test factors was continuously adjusted during the simulation process, according to the design scheme. After each simulation, the collected experimental data were analyzed by the post-processor of DEM software to output a line graph of the relationship between the number of particles breaking bonding bonds and time, as shown in Figure 4b. Using the post-processor of EDEM software, the soil particles that had shifted

position in the soil bin were counted, and this count was defined as the total number of soil particles in the working area. Ultimately, the soil breakage effect of the roller tooth can be reflected by checking the number of particles breaking bonding bonds [32].

The compaction flatness analysis of the press roller is as follows: After the simulation, in the post-processing interface of EDEM, the Selection module was used to grid the soil after work. Five cross-sections of the soil bin were selected at equal intervals along the direction of the press roller moving forward, and each cross-section was divided into several small grids of 5×10 mm, as shown in Figure 4c. By calculating the average height difference of the grid above the soil surface contour line, the average of five cross-sections was obtained as the flatness of the soil preparation for this test condition [33].

$$\begin{cases} Y_1 = \frac{N_1}{N} \times 100\% \\ Y_2 = \frac{1}{n} \sum_{i=1}^n h_i \quad (i = 1, 2, 3 \dots) \end{cases} \quad (7)$$

where, Y_1 is the breakage rate of the soil, %; N is the total number of particles in the working area, pcs; N_1 is the total number of particles breaking bonding bond in the working area, pcs; Y_2 is the flatness, mm; n is the number of grids in each row of the cross-section, pcs; and h is the height difference between the soil and the soil surface in each column, mm.

2.2.3. Field Test Program

To verify the correctness of the simulation, field experiments were conducted on the optimal parameter combination obtained from the DEM experiment, as shown in Figure 5. On 20~25 April 2022, the operational performance test of the arc-shaped tooth press device of the combined soil preparation equipment was conducted at the test demonstration base of Northeast Agricultural University. The experimental field is a dry farming area with clay loam, and the previous crop was corn. An area 200 m long and 100 m wide was selected as the test area, the average soil moisture content of the five sampling points was 14.2%, and the soil shear strength was 149.7 kPa. The test conditions at various locations on the plot are essentially the same. The test instruments mainly include the soil shear meter (50~400 kPa, accuracy 0.01 mm/min), vernier calipers (0~150 mm, accuracy 0.01 mm), tapeline, electronic scale (accuracy 0.01 g), soil ring sampling knife, and drying box.

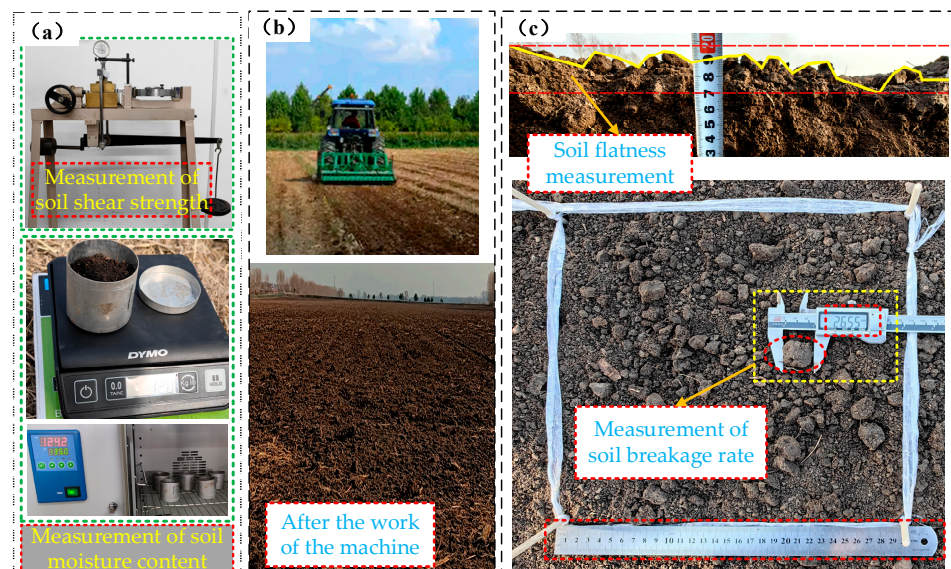


Figure 5. (a) Measurement of soil shear strength and moisture content; (b) Field test; and (c) Measurement of soil flatness and soil breakage rate.

In the field test, a tractor forward speed of $0.72\sim 1.15\text{ m}\cdot\text{s}^{-1}$, roller tooth arc length of 58.7 mm , and an ABRTVD of 37.74° were chosen. To verify the operational performance of the designed combined soil preparation equipment press device, the soil preparation performance comparative test was added with a conventional model in the same test plot, and the comparison model was a 1FY-I type profiling compactor device. The soil breakage rate and the flatness were used as evaluation indicators according to the actual situation. The measurement scheme for soil breakage rate is as follows: After the soil preparation, a square grid of 300 mm by 300 mm is taken, and the depth is the tillage depth. Soil blocks with diameters less than 25 mm in the sampling area are considered to meet the criteria for breakage soil. The percentage of soil mass that meets the requirements for breakage soil in the sampling area to the total soil mass in the same sampling area is the soil breakage rate, and the average of the five measurements is taken. The method for measuring flatness is as follows: Perpendicular to the machine's advance direction, the highest point on the ground is selected as the reference, the intercepted width is the tillage width, and the height is the tillage depth; it is divided into ten equal parts, measuring the height of each point to the ground surface. Each trip is measured five times, and the standard deviation and its average value are calculated [34]. The formulas are as follows:

$$\begin{cases} p = \frac{m_1}{m} \times 100\% \\ s_j = \sqrt{\frac{\sum_{i=1}^{n_j} (a_{ji} - a_j)^2}{n_j - 1}} \\ a_j = \frac{\sum_{i=1}^{n_j} a_{ji}}{n_j} \end{cases} \quad (8)$$

where p is the breakage rate of the soil, %; m_1 is the mass of clod diameter less than 25 mm in the sampling area, g; m is the total soil mass in the sampling area, g; a_j is the mean soil flatness of the j -th trip, mm; a_{ji} is the measured value of the i -th soil flatness of the j -th trip, mm; n_j is the number of the j -th trip test points, pcs; and s_j is the standard deviation of the j -th trip soil flatness, mm.

3. Results and Discussion

The simulation tests were completed according to the design scheme provided in Design-Expert 8.0.6. The results are shown in Table 6, including 14 analysis factors and 9 null tests for estimation errors. An analysis of variance (ANOVA) on the test results was performed by applying Design-Expert 8.0.6 software, and the results are shown in Table 7. An F-test was carried out at the confidence level of 0.1, and the regression square and degree of freedom of the insignificant interaction term were incorporated into the residual term. The reliability of the multiple linear regression model was verified by the internally studentized residuals analysis of the soil breakage rate and flatness, as shown in Figures 6a and 6b, respectively. The regression model equations for the evaluation indexes are obtained as Equation (9).

$$\begin{cases} Y_1 = 93.08 + 0.71x_1 + 0.24x_2 - 0.23x_3 + 0.36x_1x_2 + 0.59x_2x_3 - 0.32x_2^2 - 0.30x_3^2 \\ Y_2 = 23.36 + 1.22x_1 - 2.47x_2 - 1.15x_3 - 1.50x_1x_2 - 2.25x_1x_3 + 1.38x_1^2 - 1.98x_2^2 - 3.75x_3^2 \end{cases} \quad (9)$$

3.1. Analysis of ANOVA

The regression coefficients in the regression models for each evaluation index were subjected to ANOVA. According to the misfit values of the regression models for each evaluation index in Table 7, we can see that $P_{L1} = 0.5352 > 0.1$ and $P_{L2} = 0.3510 > 0.1$ (both insignificant), indicating no attrition factor in the regression analysis, and that the regression models fit better. The model values $P_{M1} < 0.0001$ and $P_{M2} < 0.0001$ for the regression models (both highly significant) indicate that the regression results have a certain degree of reliability.

Table 6. Test schemes and results.

Test Number	Factor			Evaluation Index	
	x_1	x_2	x_3	$Y_1/\%$	Y_2/mm
1	−1.000	−1.000	−1.000	92.6	18
2	1.000	−1.000	−1.000	93.5	27
3	−1.000	1.000	−1.000	91.4	13
4	1.000	1.000	−1.000	93.5	18
5	−1.000	−1.000	1.000	91.6	19
6	1.000	−1.000	1.000	91.5	21
7	−1.000	1.000	1.000	92.5	19
8	1.000	1.000	1.000	94.1	13
9	−1.682	0.000	0.000	91.5	26
10	1.682	0.000	0.000	94.6	30
11	0.000	−1.682	0.000	91.7	22
12	0.000	1.682	0.000	92.3	15
13	0.000	0.000	−1.682	92.6	17
14	0.000	0.000	1.682	91.5	10
15	0.000	0.000	0.000	93.5	24
16	0.000	0.000	0.000	92.5	22
17	0.000	0.000	0.000	92.7	21
18	0.000	0.000	0.000	93.2	25
19	0.000	0.000	0.000	93.6	21
20	0.000	0.000	0.000	92.5	25
21	0.000	0.000	0.000	93.3	23
22	0.000	0.000	0.000	92.9	24
23	0.000	0.000	0.000	93.3	25

Table 7. ANOVA results.

Source of Variation	Y_1					Y_2				
	Sum of Squares	Degree of Squares	Mean Square	F	p	Sum of Squares	Degree of Squares	Mean Square	F	p
Model	15.6	9	74	10.20	0.0001 ***	500.7	9	55.64	18.47	<0.0001 ***
x_1	6.9	1	6.91	40.63	<0.0001 ***	20.49	1	20.49	6.80	0.0217 **
x_2	0.8	1	0.80	4.72	0.0490 **	83.5	1	83.52	27.72	0.0002 ***
x_3	0.73	1	0.73	4.27	0.0592	18.22	1	18.22	6.05	0.0287 **
x_1x_2	1.05	1	1.05	6.18	0.0273 **	18.00	1	18.00	5.98	0.0295 **
x_1x_3	0.28	1	0.28	1.65	0.2208	40.5	1	40.5	13.44	0.0028 ***
x_2x_3	2.76	1	2.76	16.24	0.0014 ***	4.50	1	4.50	1.49	0.2433
x_1^2	0.044	1	0.044	0.26	0.6204	30.30	1	30.30	10.06	0.0074 ***
x_2^2	1.61	1	1.61	9.49	0.0088 ***	62.16	1	62.16	20.64	0.0006 ***
x_3^2	1.44	1	1.44	8.47	0.0122 **	222.93	1	222.93	74.00	<0.0001 ***
Residual	0.8	5	0.16			17.16	5	3.43		
Lack of fit	1.40	8	0.18	0.92	0.5132	22.00	8	2.75	1.25	0.3709
Corrected total	17.83	22				539.91	22			

Note: “****” indicates highly significant ($p < 0.01$) and “***” indicates significant ($0.01 < p < 0.05$).

The results obtained through an analysis of variance and the fitting of experimental data are shown in Table 6. The analysis of soil breakage rate indicates that x_1 , x_2x_3 , and x_2^2 have a highly significant effect on the soil breakage rate ($p < 0.01$); x_2 , x_1x_2 , and x_3^2 have a significant effect on the soil breakage rate ($0.01 < p < 0.05$); x_3 has a more significant effect on the soil breakage rate ($0.05 < p < 0.1$); and the rest of the test factors have no significant effect on the soil breakage rate ($p > 0.1$). The analysis of flatness indicates that x_2 , x_1x_3 , x_1^2 , x_2^2 , and x_3^2 have a highly significant ($p < 0.01$) effect on the flatness; x_1 , x_3 , and x_1x_2 have a significant ($0.01 < p < 0.05$) effect on the flatness; and the rest of the test factors have a non-significant ($p > 0.1$) effect on the flatness.

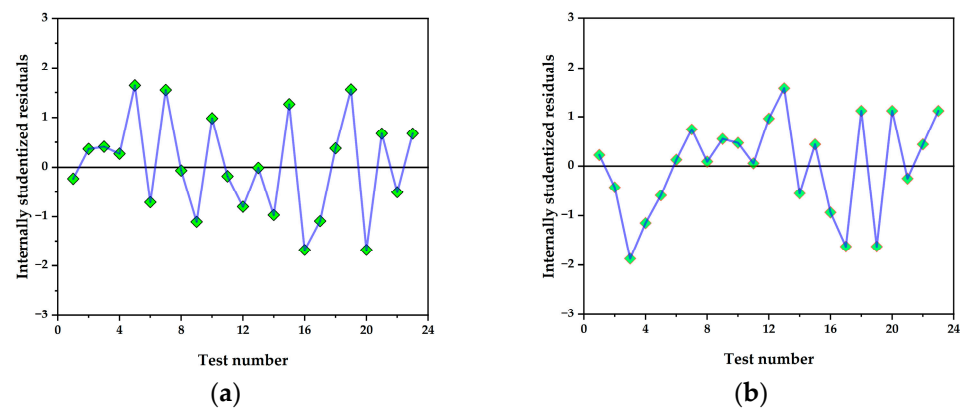


Figure 6. (a) Internally studentized residual analysis of soil breakage rate. (b) Internally studentized residual analysis of flatness.

3.2. Field Test

To verify the accuracy of the DEM simulation tests, the press device that was designed based on the optimized parameter combination was applied to field performance verification tests. These results are shown in Table 8.

Table 8. Comparison of test results with different machines.

Type	Soil Breakage Rate/%	Flatness Value/mm
Arc-shaped tooth	95.6	20.6
1FY-I type	92.2	31.8
Comparison	Upgraded by 3.4	Reduced by 11.2

From the obtained experimental data, it can be seen that the optimized operation parameter combination of the press device shows good operation performance. The test result of flatness was basically consistent with the simulation result, and the test result of the soil breakage rate was higher than the simulation result, but was within the allowable range. This may be because the soil breakage rate is calculated in the simulation process by counting the number of breakage bonding bonds between particles, which is guaranteed to exist between all particles when generating the particles. Whereas in the field test, the soil breakage rate is determined by the weight of clods that are less than 25 mm in diameter after soil preparation work. Hence, the soil breakage rate obtained in the simulation is lower than that of the field test. The field test results show that the established DEM model and the virtual simulation optimization test have accuracy and validity, and the optimized parameter combination is credible.

3.3. The Impact of Each Factor on the Performance Evaluation Index

To express the influence of each factor on the evaluation indexes more clearly and explicitly, the quadratic regression equations of the two evaluation indexes mentioned above are reduced in dimensionality. The effect of the forward speed and the roller tooth arc length on the soil breakage rate when the ABRTVD is 37° is shown in Figure 7a. When the forward speed is constant, as the arc length of the roller tooth increases, the soil breakage rate shows a trend of first increasing and then decreasing; when selecting an optimal forward speed of $1.1 \text{ m}\cdot\text{s}^{-1}$, the soil breakage rate shows a trend of first increasing and then decreasing with the increase in roller tooth arc length, and the optimal range of roller tooth arc length is 56~59 mm. The soil breakage rate increases with the increase in forward speed and the increasing trend gradually flattens out, and the optimal forward speed range is $0.72\sim 1.50 \text{ m}\cdot\text{s}^{-1}$.

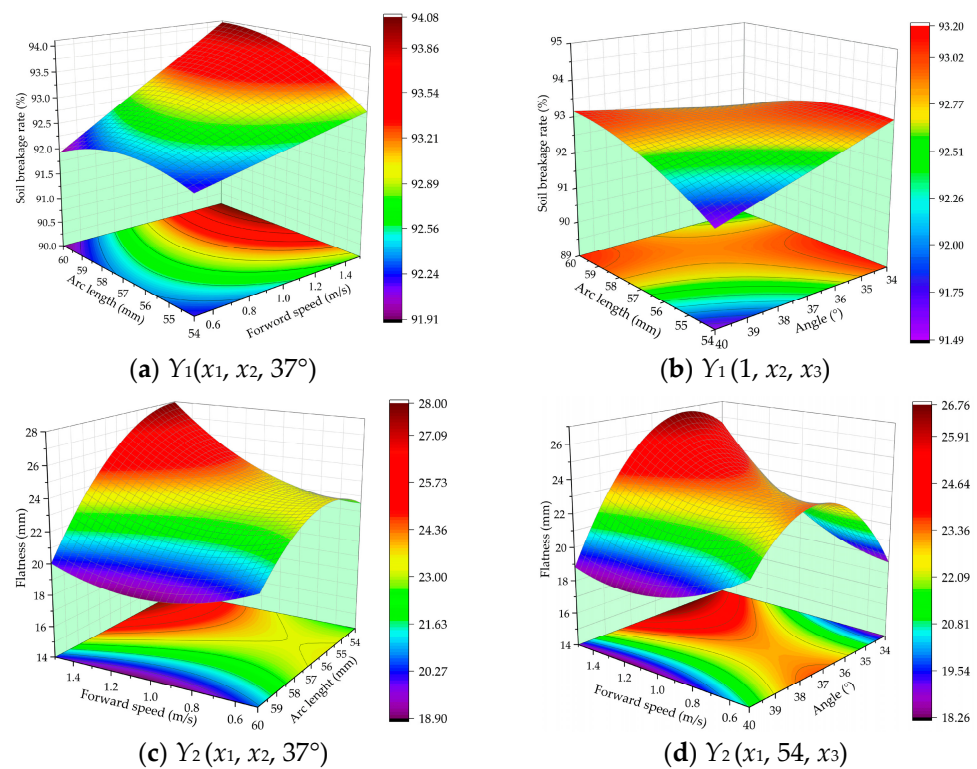


Figure 7. (a) The effect of the interaction of forward speed and roller tooth arc length on soil breakage rate; (b) The effect of the interaction of roller tooth arc length and the ABRTVD on soil breakage rate; (c) The effect of the interaction of forward speed and roller tooth arc length on flatness; (d) The effect of the interaction of forward speed and the ABRTVD on flatness.

The effect of the roller tooth arc length and the ABRTVD on the soil breakage rate when the forward speed is $1 \text{ m}\cdot\text{s}^{-1}$ is shown in Figure 7b. When the roller tooth arc length is small, the soil breakage rate decreases with the increase in the ABRTVD; when the roller tooth arc length is large, the soil breakage rate increases with the increase in the ABRTVD, and the optimal value of the ABRTVD is 35~38 mm. When the ABRTVD is small, the soil breakage rate tends to decrease as the roller tooth arc length increases; when the ABRTVD is large, the soil breakage rate tends to increase with the increase in the roller tooth arc length, and the optimum roller tooth arc length range is 55~59 mm.

When the ABRTVD is 37° , the effect of the forward speed and the roller tooth arc length on the flatness is shown in Figure 7c. When the arc length of roller tooth is small, the flatness value increases with the increase in the forward speed; when the arc length of roller tooth is large, the flatness value first decreases and then increases with the increase in the forward speed, and the optimal forward speed range is $0.70\sim 1.30 \text{ m}\cdot\text{s}^{-1}$; and when the forward speed is constant, the flatness value tends to first increase and then decrease as the arc length of roller tooth increases, and the optimal range of roller tooth arc length is 56~60 mm.

The effect of the forward speed and the ABRTVD on the flatness when the arc length of the roller tooth is 54 mm is shown in Figure 7d. When the forward speed is constant, as the ABRTVD increases, the flatness value tends to first increase and then decrease, and the optimal angle range is $37\sim 40^\circ$. When the ABRTVD is constant, as the forward speed

increases, the flatness value tends to first decrease and then increase, and the optimal forward speed is $0.70\sim 1.15\text{ m}\cdot\text{s}^{-1}$.

$$\begin{cases} \max Y_1(x_1, x_2, x_3) \\ \min Y_2(x_1, x_2, x_3) \\ \text{s.t.} \begin{cases} 0.72\text{m}\cdot\text{s}^{-1} \leq x_1 \leq 1.15\text{m}\cdot\text{s}^{-1} \\ 56\text{mm} \leq x_2 \leq 59\text{mm} \\ 37^\circ \leq x_3 \leq 40^\circ \end{cases} \end{cases} \quad (10)$$

By analyzing the four response surface plots in Figure 7, the optimal range of the horizontal combinations of experimental factors was obtained, as shown in Equation (10). The four regression models were solved by using the optimization module in the Design-Expert 8.0.6 software. According to the actual working requirements of the press device and the results of the above model analysis, the comprehensive operating performance of machine is ideal when the forward speed is $0.72\sim 1.15\text{ m}\cdot\text{s}^{-1}$, the arc length of roller tooth is 58.7 mm, and the ABRTVD is 37.74° . The predicted soil breakage rate is 93.62%, and the flatness is 20.73 mm. By conducting discrete element simulation experiments on this set of data, it was found that the soil breakage rate is 93.58% and the flatness is 21.06 mm, which are generally consistent with the optimization results within the error tolerance.

4. Conclusions

In this study, an arc-shaped tooth press device used in conjunction with combined soil preparation equipment for potatoes was designed and analyzed, and its performance through discrete element simulation experiments and field tests was explored. The conclusions are as follows:

- (1) An arc-shaped tooth press device was designed to match the combined soil preparation equipment, and the overall structure and working principle of the combined soil preparation equipment are illustrated; the press roller, as a key component of press device, was analyzed for its working force on the soil; the static and dynamic forces of the arc-shaped tooth welded on the roller were analyzed, and the shear stress equation of tooth cutting soil was constructed; and the key factors affecting the magnitude of shear stress were determined and their range were solved by using MATLAB;
- (2) Design-Expert 8.0.6 software was used for the test design, recording the forward speed, the roller tooth arc length, and the ABRTVD as test factors, as well as the soil breakage rate and flatness as test indexes. On the basis of SolidWorks modeling, a press roller-soil simulation model was established using EDEM software, and a quadratic regression orthogonal rotation simulation experiment with three-factor and five-level was conducted on the working process of the press roller. A regression mathematical model was established between various experimental factors and experimental indexes, and the optimal parameters combination for the arc-shaped tooth press device was obtained as follows: the tractor forward speed is $0.72\sim 1.15\text{ m}\cdot\text{s}^{-1}$, the roller tooth arc length is 58.7 mm, the ABRTVD is 37.74° , the predicted soil breakage rate is 93.62%, and the flatness is 20.73 mm; simulation verification was conducted on the optimal combination parameters, and it was found that the soil breakage rate under this set of parameters was 93.58% and the flatness was 21.06 mm, which is basically consistent with the optimization results. The feasibility of the DEM to analyze the operational performance of a press device in clay loam was verified, and this provided a new method for later research on press devices;
- (3) Field tests were conducted using the optimal combination parameters obtained through analysis; after the operation of the arc-shaped tooth press device of the combined soil preparation machine, the soil breakage rate is 95.6%, the flatness is 20.6 mm, and the operational performance is better than that of the traditional press device. From the perspective of combining theoretical analysis and experiments,

a compaction device for a potato joint soil preparation machine was designed in this article, and this broadens the research approach for traditional combined soil preparation machines that only focus on soil breakage devices. This device meets the quality requirements for soil preparation before potato planting, which is beneficial for improving the quality of potato emergence after sowing and thus increasing potato yield.

Author Contributions: Conceptualization, Z.Z., X.Z. and J.L. (Jicheng Li); methodology, Z.Z., X.Z. and J.L. (Jicheng Li); software, Z.Z. and Y.Q.; validation, Z.Z., J.L. (Jinqing Lyu) and J.L. (Jicheng Li); investigation, Z.Z. and J.L. (Jinni Liu); resources, J.L. (Jicheng Li); data curation, Z.Z. and X.Z.; writing—original draft preparation, Z.Z.; writing—review and editing, X.Z. and J.L. (Jicheng Li); supervision, J.L. (Jinqing Lyu). All authors have read and agreed to the published version of the manuscript.

Funding: This research was funded by the Special Program for Scientists in China Agriculture Research System (grant number: CARS-09-P23) and the Opening Project of the Northern Potato Full Mechanization Research Base (Northeast China) of the Ministry of Agriculture and Rural Affairs (grant number: BM-QCJXH2201).

Institutional Review Board Statement: Not applicable.

Informed Consent Statement: Not applicable.

Data Availability Statement: All data are presented in this article in the form of figures and tables.

Acknowledgments: The authors would like to acknowledge the College of Engineering at Northeast Agricultural University and the Northern Potato Full Mechanization Research Base (Northeast China) of the Ministry of Agriculture and Rural Affairs.

Conflicts of Interest: The authors declare no conflict of interest.

References

1. Singh, P.; Sandhu, A.S. Energy budgeting and economics of potato (*Solanum tuberosum* L.) cultivation under different sowing methods in north-western India. *Energy* **2023**, *269*, 986–993. [[CrossRef](#)]
2. Zhang, Q.; Wang, S.; Sun, Y.; Zhang, Y.; Li, H.; Liu, P.; Wang, X.; Wang, R.; Li, J. Conservation tillage improves soil water storage, spring maize (*Zea mays* L.) yield and WUE in two types of seasonal rainfall distributions. *Soil Tillage Res.* **2021**, *215*, 105237. [[CrossRef](#)]
3. Tang, H.; Xu, C.; Xu, W.; Xu, Y.; Xiang, Y.; Wang, J. Method of straw ditch-buried returning, development of supporting machine and analysis of influencing factors. *Front. Plant Sci.* **2022**, *13*, 967838. [[CrossRef](#)] [[PubMed](#)]
4. Lyu, J.; Yi, S.; Tao, G.; Tao, G.; Mao, X. Parameter optimization and experiment of splitter sliding-knife opener for potato planter. *Trans. CSAE.* **2018**, *34*, 44–54. (In Chinese)
5. Kazlauskas, M.; Šarauskius, E.; Lekavičienė, K.; Naujokienė, V.; Romanekas, K.; Bručienė, I.; Buragienė, S.; Steponavičius, D. The Comparison Analysis of Uniform-and Variable-Rate Fertilizations on Winter Wheat Yield Parameters Using Site-Specific Seeding. *Processes* **2022**, *10*, 2717. [[CrossRef](#)]
6. Mileusnić, Z.I.; Saljnikov, E.; Radojević, R.L.; Petrović, D.V. Soil compaction due to agricultural machinery impact. *J. Terramech.* **2022**, *100*, 51–60. [[CrossRef](#)]
7. Vilakazi, B.S.; Zengeni, R.; Mafongoya, P. Selected Soil Physicochemical Properties under Different Tillage Practices and N Fertilizer Application in Maize Mono-Cropping. *Agriculture* **2022**, *12*, 1738. [[CrossRef](#)]
8. Matin, M.A.; Hossain, M.I.; Gathala, M.K.; Timsina, J.; Krupnik, T.J. Optimal design and setting of rotary strip-tiller blades to intensify dry season cropping in Asian wet clay soil conditions. *Soil Tillage Res.* **2021**, *207*, 104854. [[CrossRef](#)]
9. Lee, K.S.; Park, S.H.; Park, W.Y.; Lee, C.S. Strip tillage characteristics of rotary tiller blades for use in a dryland direct rice seeder. *Soil Tillage Res.* **2003**, *71*, 25–32. [[CrossRef](#)]
10. Zhao, J.; Wang, A.; Ma, Y.; Li, J.; Hao, J.; Nie, Q.; Long, S.; Yang, Q. Design and test of soil preparation machine combined subsoiling, rotary tillage and soil breaking. *Trans. CSAE.* **2019**, *35*, 46–54. (In Chinese)
11. Kang, D.; Sun, W.; Zhang, T.; Li, D.; Wu, J. Study and experiment on subsoiling, stubble-breaking and pressing soil combined tillage machine in arid area. *Trans. J. China Agric. Univ.* **2018**, *23*, 133–142. (In Chinese)
12. Chen, G.; Dong, C.; Zhang, L.; Wang, Q.; He, J.; Long, H. Design and experiment of shajiang black soil preparation machine with double pressing roller. *Trans. Chin. Soc. Agric. Mach.* **2022**, *53*, 50–59. (In Chinese)
13. Dai, F.; Song, X.; Zhao, W.; Wie, W.; Zhang, F.; Ma, H. Design and Experiment of Operation Machine for Filming and Covering Soil on Tiny Ridges. *Trans. Chin. Soc. Agric. Mach.* **2020**, *3*, 97–105+129. (In Chinese)

14. Zhao, S.; Liu, H.; Tan, H.; Yang, Y.; Zhang, X. Design and Experiment of Bidirectional Profiling Press Device for Hilly Area. *Trans. Chin. Soc. Agric. Mach.* **2017**, *48*, 82–89.
15. Okayasu, T.; Morishita, K.; Terao, H.; Mitsuoka, M.; Inoue, E.; Fukami, K. Modeling and prediction of soil cutting behavior by a plow frictional slider. *Int. Conf. Agric. Eng. CIGR Ageng.* **2012**, *23*, 23.
16. Kim, Y.S.; Siddique, M.; Kim, W.S.; Kim, Y.J.; Lim, R.G. DEM simulation for draft force prediction of moldboard plow according to the tillage depth in cohesive soil. *Comput. Electron. Agric.* **2021**, *189*, 106368. [[CrossRef](#)]
17. Zhang, G.; Zhang, Z.; Xiao, M.; Pb, B.; Bartos, P.; Bohata, A. Soil-cutting simulation and parameter optimization of rotary blade's three-axis resistances by response surface method. *Comput. Electron. Agric.* **2019**, *164*, 104902. [[CrossRef](#)]
18. Barbosa, L.A.P. Modelling the aggregate structure of a bulk soil to quantify fragmentation properties and energy demand of soil tillage tools in the formation of seedbeds. *Biosyst. Eng.* **2020**, *197*, 203–215. [[CrossRef](#)]
19. Du, J.; Heng, Y.; Zheng, K.; Zhang, W.; Zhang, J.; Xia, J. Evaluation of the Performance of a Combined Tillage Implement with Plough and Rotary Tiller by Experiment and DEM Simulation. *Processes* **2021**, *9*, 1174. [[CrossRef](#)]
20. Jin, H.; Hongwen, L.I.; Haitao, C.H.E.N.; Caiyun, L.U.; Qingjie, W.A.N.G. Research progress of conservation tillage technology and machine. *Trans. Chin. Soc. Agric. Mach.* **2018**, *49*, 1–19. (In Chinese)
21. Blevins, R.L.; Smith, M.S.; Thomas, G.W.; Frye, W.W. Influence of conservation tillage on soil properties. *J. Soil Water Conserv.* **1983**, *38*, 301–305.
22. De Oliveira, I.N.; de Souza, Z.M.; Bolonhezi, D.; Totti, M.C.V.; de Moraes, M.T.; Lovera, L.H.; de Souza Lima, E.; Esteban, D.A.A.; Oliveira, C.F. Tillage systems impact on soil physical attributes, sugarcane yield and root system propagated by pre-sprouted seedlings. *Soil Tillage Res.* **2022**, *223*, 105460. [[CrossRef](#)]
23. China Academy of Agricultural Mechanization Science. *Handbook of Agricultural Machinery Design*; China Agricultural Science and Technology Press: Beijing, China, 2007.
24. Luo, X.W.; Perumpral, J.V. Study on soil strength with microwave reflection loss. *Trans. CSAE.* **1995**, *11*, 46–51. (In Chinese)
25. Lapen, D.R.; Hayhoe, H.N.; Topp, G.C.; McLaughlin, N.B.; Gregorich, E.G.; Curnoe, W.E. Measurements of mouldboard plow draft: II Draft-soil-srop and yield-draft association. *Precis. Agric.* **2002**, *3*, 237–257. [[CrossRef](#)]
26. Hou, S.; Wang, S.; Ji, Z.; Zhu, X. Design and Test of the Clearing and Covering of a Minimum-Tillage Planter for Corn Stubble. *Agriculture* **2022**, *12*, 1209. [[CrossRef](#)]
27. Tang, H.; Xu, C.; Zhao, J.; Wang, J. Stripping mechanism and loss characteristics of a stripping-prior-to-cutting header for rice harvesting based on CFD-DEM simulations and bench experiments. *Biosyst. Eng.* **2023**, *229*, 116–136. [[CrossRef](#)]
28. Mousaviraad, M.; Tekeste, M.; Rosentrater, K.A. Calibration and Validation of a Discrete Element Model of Corn Using Grain Flow Simulation in a Commercial Screw Grain Auger. *Trans. ASABE* **2017**, *60*, 1403–1415. (In Chinese) [[CrossRef](#)]
29. Tang, H.; Xu, F.D.; Xu, C.S.; Zhao, J.L.; Wang, Y.-J. The influence of a seed drop tube of the inside-filling air-blowing precision seed-metering device on seeding quality. *Comput. Electron. Agric.* **2023**, *204*, 107555. [[CrossRef](#)]
30. Tian, X.; Cong, X.; Qi, J.; Guo, H.; Li, M.; Fan, X. Parameter calibration of discrete element model for corn straw–soil mixture in black soil areas. *Trans. Chin. Soc. Agric. Mach.* **2021**, *52*, 100–108.
31. Tang, H.; Xu, C.; Wang, Z.; Wang, Q.; Wang, J. Optimized Design, Monitoring System Development and Experiment for a Long-Belt Finger-Clip Precision Corn Seed Metering Device. *Front. Plant Sci.* **2022**, *13*, 814747. [[CrossRef](#)]
32. Lyu, J.; Liu, Q.; Yang, D.; Li, J.; Liu, Z. Design and Test of Key Components of Ploughshare Potato Field Cultivator in Sandy Loam. *Trans. Chin. Soc. Agric. Mach.* **2021**, *52*, 27–39. (In Chinese)
33. Sun, J.; Wang, Y.; Ma, Y.; Tong, J.; Zhang, Z. DEM simulation of bionic subsoilers (tillage depth > 40 cm) with drag reduction and lower soil disturbance characteristics. *Adv. Eng. Softw.* **2018**, *119*, 30–37. [[CrossRef](#)]
34. Qin, K.; Ding, W.; Fang, Z.; Du, T.; Zhao, S.; Wang, Z. Design and experiment of plowing and rotary tillage combined machine. *Trans. CSAE.* **2016**, *32*, 7–16. (In Chinese)

Disclaimer/Publisher's Note: The statements, opinions and data contained in all publications are solely those of the individual author(s) and contributor(s) and not of MDPI and/or the editor(s). MDPI and/or the editor(s) disclaim responsibility for any injury to people or property resulting from any ideas, methods, instructions or products referred to in the content.